AMERICAN SOCIETY FOR MICROBIOLOGY | Journal of Virology®

VIRUS-CELL INTERACTIONS

Species-Specific Pathogenicity of Severe Fever with Thrombocytopenia Syndrome Virus Is Determined by Anti-STAT2 Activity of NSs

Rokusuke Yoshikawa,[a,b] Saori Sakabe,[a,c] Shuzo Urata,[a,b] Jiro Yasuda[a,b,c]

[a]Department of Emerging Infectious Diseases, Institute of Tropical Medicine (NEKKEN), Nagasaki University, Nagasaki, Japan
[b]National Research Center for the Control and Prevention of Infectious Diseases (CCPID), Nagasaki University, Nagasaki, Japan
[c]Graduate School of Biomedical Sciences and Program for Nurturing Global Leaders in Tropical and Emerging Communicable Diseases, Nagasaki University, Nagasaki, Japan

ABSTRACT Severe fever with thrombocytopenia syndrome virus (SFTSV) is a novel emerging virus that has been identified in China, South Korea, and Japan, and it induces thrombocytopenia and leukocytopenia in humans with a high case fatality rate. SFTSV is pathogenic to humans, while immunocompetent adult mice and golden Syrian hamsters infected with SFTSV never show apparent symptoms. However, mice deficient for the gene encoding the α chain of the alpha- and beta-interferon receptor (*Ifnar1*$^{-/-}$ mice) and golden Syrian hamsters deficient for the gene encoding signal transducer and activator of transcription 2 (*Stat2*$^{-/-}$ hamsters) are highly susceptible to SFTSV infection, with infection resulting in death. The nonstructural protein (NSs) of SFTSV has been reported to inhibit the type I IFN response through sequestration of human STAT proteins. Here, we demonstrated that SFTSV induces lethal acute disease in STAT2-deficient mice but not in STAT1-deficient mice. Furthermore, we discovered that NSs cannot inhibit type I IFN signaling in murine cells due to an inability to bind to murine STAT2. Taken together, our results imply that the dysfunction of NSs in antagonizing murine STAT2 can lead to inefficient replication and the loss of pathogenesis of SFTSV in mice.

IMPORTANCE Severe fever with thrombocytopenia syndrome (SFTS) is an emerging infectious disease caused by SFTSV, which has been reported in China, South Korea, and Japan. Here, we revealed that mice lacking STAT2, which is an important factor for antiviral innate immunity, are highly susceptible to SFTSV infection. We also show that SFTSV NSs cannot exert its anti-innate immunity activity in mice due to the inability of the protein to bind to murine STAT2. Our findings suggest that the dysfunction of SFTSV NSs as an IFN antagonist in murine cells confers a loss of pathogenicity of SFTSV in mice.

KEYWORDS NSs, SFTSV, STAT2, animal model, mouse

Severe fever with thrombocytopenia syndrome (SFTS) is an emerging infectious disease caused by the SFTS virus (SFTSV), which is a novel *Phlebovirus* of the *Phenuiviridae* family. SFTSV was first isolated in rural areas of central China in 2011 and subsequently identified in South Korea and Japan (1–4). Moreover, another emerging phlebovirus genetically close to SFTSV, Hartland virus, was found in the United States (5). SFTS is clinically characterized by fever, vomiting, diarrhea, thrombocytopenia, leukocytopenia, and elevated serum levels of enzymes, such as creatine kinase (CK), aspartate aminotransferase (AST), alanine transaminase (ALT), and lactate dehydrogenase (LDH) (6–8). However, the pathogenesis of SFTSV in humans is still poorly

Citation Yoshikawa R, Sakabe S, Urata S, Yasuda J. 2019. Species-specific pathogenicity of severe fever with thrombocytopenia syndrome virus is determined by anti-STAT2 activity of NSs. J Virol 93:e02226-18. https://doi.org/10.1128/JVI.02226-18.

Editor Rebecca Ellis Dutch, University of Kentucky College of Medicine

Copyright © 2019 American Society for Microbiology. All Rights Reserved.

Address correspondence to Jiro Yasuda, j-yasuda@nagasaki-u.ac.jp.

R.Y. and S.S. contributed equally to this work.

Received 12 December 2018
Accepted 14 February 2019
Accepted manuscript posted online 27 February 2019
Published 1 May 2019

understood, and no effective vaccines or antiviral drugs are currently available for treatment of SFTS.

The SFTSV genome is composed of three negative-strand RNA segments (S, M, and L). The L segment encodes the viral RNA-dependent RNA polymerase (L), the M segment encodes the glycoprotein precursors (Gn and Gc), and the S segment encodes the nucleocapsid protein (N) and nonstructural protein (NSs).

The innate immune response, including the type I interferon (IFN) response, is important for preventing viral infection (9). Antiviral innate immunity is initiated by the recognition of viral infection through cellular pattern recognition receptors (PRRs), such as transmembrane toll-like receptor 3 (TLR3), cytosolic RIG-I-like receptors, and MDA5 (10). Upon recognition, this signal cascade leads to the induction of type I IFN. The activation of the IFN signaling pathway by the binding of secreted IFN to IFN receptors results in the phosphorylation of STAT1 and STAT2. The heterodimer or homodimer of phosphorylated STAT forms heterotrimeric interferon-stimulated gene factor 3 (ISGF3) with IRF-9. The translocation of ISGF3 into the cell nucleus results in the activation of antiviral IFN-stimulated genes (ISGs) by its binding to an IFN-stimulated response element (ISRE) (11). However, during a phlebovirus infection, viral NSs is thought to play a major role in repressing the innate immune response by targeting the IFN response pathway as an IFN antagonist (12–15). Previous studies have reported that NSs of SFTSV inhibits type I and III IFN responses through sequestration of human STAT2 protein in viral replication complexes (13–15).

SFTSV infections do not cause severe disease in immunocompetent mice and golden Syrian hamsters, while type I IFN receptor knockout (*Ifnar1*$^{-/-}$) mice, which lack the gene encoding the α chain of the IFN-α and -β receptor, and STAT2-deficient golden Syrian hamsters are highly susceptible to SFTSV, with infection resulting in death (16–19). This suggests that efficient replication of SFTSV in mice and hamsters is prevented by antiviral innate immunity and that NSs of SFTSV does not inhibit IFN signaling in murine and hamster cells. STAT1 and STAT2 are important factors for antiviral innate immunity. However, the relationship between SFTSV pathogenicity and STAT function remains unknown. In this study, to investigate the role of STAT1 and STAT2 in the pathogenesis and replication of SFTSV in mice, we examined the pathogenicity of SFTSV in *Stat1*$^{-/-}$ and *Stat2*$^{-/-}$ mice and measured the antagonistic activities of NSs against IFN signaling in murine cells.

RESULTS

SFTSV infection to *Ifnar1*$^{-/-}$ mice. It has been reported that *Ifnar1*$^{-/-}$ mice are highly susceptible to SFTSV strains YL-1 and SPL010, with infection resulting in death (16–17). In this study, we used the YG-1 strain isolated from the first SFTS patient reported in Japan (4). Wild-type C57BL/6 mice and *Ifnar1*$^{-/-}$ mice were intradermally (i.d.) inoculated with 10 focus-forming units (FFU) of the SFTSV (YG-1). All infected wild-type mice survived without any clinical signs (Fig. 1A). In contrast, all infected *Ifnar1*$^{-/-}$ mice died 5 to 8 days after infection (Fig. 1A). Moreover, all *Ifnar1*$^{-/-}$ mice infected with SFTSV showed severe body weight loss, leukocytopenia, and thrombocytopenia 1 to 7 days postinfection (p.i.) (Fig. 1B to D). The titers of SFTSV in the organs (brains, lungs, livers, spleens, kidneys, and intestines) and plasma of infected *Ifnar1*$^{-/-}$ and wild-type mice were also measured by focus-forming assay at 3, 5, and 7 days p.i. As shown in Fig. 2, efficient viral replication in *Ifnar1*$^{-/-}$ mice was observed in the spleen and plasma at 3 days p.i., all organs at 5 days p.i., and the spleen, kidney, and intestine at 7 days p.i. In contrast, we could not detect infectious SFTSV in the plasma or organs of wild-type mice.

The results show that SFTSV (YG-1) induces lethal acute infection accompanied by thrombocytopenia in *Ifnar1*$^{-/-}$ mice.

SFTSV causes lethal infection in *Stat2*$^{-/-}$mice but not *Stat1*$^{-/-}$ mice. To investigate the roles of STAT1 and STAT2 in SFTSV infection, *Stat1*$^{-/-}$, *Stat2*$^{-/-}$, and *Ifnar1*$^{-/-}$ mice next were infected with the YG-1 strain. None of the infected *Stat2*$^{-/-}$ mice survived, while all of the *Stat1*$^{-/-}$ mice infected with YG-1 survived (Fig. 1A). As

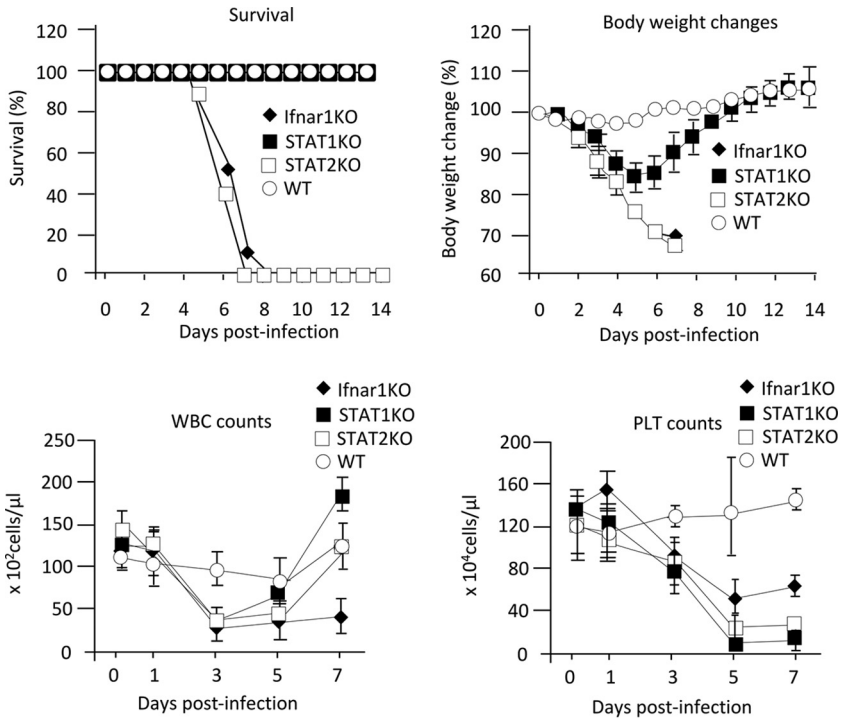

FIG 1 Clinical pathologies of mice infected with SFTSV. Wild-type C57BL/6 (WT), *Ifnar1*$^{-/-}$, *Stat1*$^{-/-}$, and *Stat2*$^{-/-}$ mice were infected with 10 FFU of SFTSV (YG1). Survival (A) and body weight (B) changes were observed daily for 14 days p.i. ($n = 10$). For WBC and PLT counts, blood samples were collected from two male and three female mice at 0, 1, 3, 5, and 7 days p.i. The values are shown as means ± standard deviations (SDs).

shown in Fig. 1B, *Stat2*$^{-/-}$ mice lost body weight at 1 to 7 days p.i., while *Stat1*$^{-/-}$ mice lost body weight at 1 to 5 days p.i. and then recovered. Unlike in *Ifnar1*$^{-/-}$ mice, the number of white blood cells in *Stat1*$^{-/-}$ and *Stat2*$^{-/-}$ mice transiently decreased after infection and then recovered to normal values (Fig. 1C). Both *Stat1*$^{-/-}$ and *Stat2*$^{-/-}$ mice infected with SFTSV showed thrombocytopenia regardless of survival (Fig. 1D). This implies that the lethality of SFTSV is not associated with thrombocytopenia. We next measured the titers of SFTSV in organs (brains, lungs, livers, spleens, kidneys, and intestines) and plasma of infected *Stat1*$^{-/-}$ and *Stat2*$^{-/-}$ mice by focus-forming assay at 3, 5, and 7 days p.i. In *Stat2*$^{-/-}$ mice, SFTSV was detected in the plasma, spleen, and kidney at 3 days p.i., the plasma and all organs at 5 days p.i., and the spleen and kidney at 7 days p.i. In *Stat1*$^{-/-}$ mice, SFTSV replicated in the lung, spleen, kidney, intestine, and plasma; however, the maximum titers of SFTSV in these organs and plasma were lower than those in *Stat2*$^{-/-}$ mice (Fig. 2).

These results indicate that *Stat2*$^{-/-}$ and *Ifnar1*$^{-/-}$ mice, but not *Stat1*$^{-/-}$ mice, are highly susceptible to SFTSV infection, which suggests that STAT2 plays a critical role in the suppression of SFTSV replication in mice.

SFTSV NSs cannot suppress type I IFN signaling in murine cells. It has been reported that SFTSV suppresses type I IFN signaling in human cells (13). Therefore, we hypothesized that SFTSV cannot suppress type I IFN signaling in murine cells, and IFN-mediated innate immunity restricts SFTSV replication in mice. To address this possibility, the ISRE activation by SFTSV infection was examined in human-derived HEK293T cells and mouse-derived NIH 3T3 cells using dual-luciferase reporter (DLR) gene assay. As shown in Fig. 3A, SFTSV infection did not induce the ISRE activation in HEK293T cells, while the ISRE activation was induced by SFTSV infection in NIH 3T3 cells. These results suggest that SFTSV cannot inhibit type I IFN signaling in murine cells.

Recently, SFTSV NSs has been reported to function as an IFN antagonist (13–15). Therefore, the effects of NSs on ISRE activation in HEK293T cells and NIH 3T3 cells were

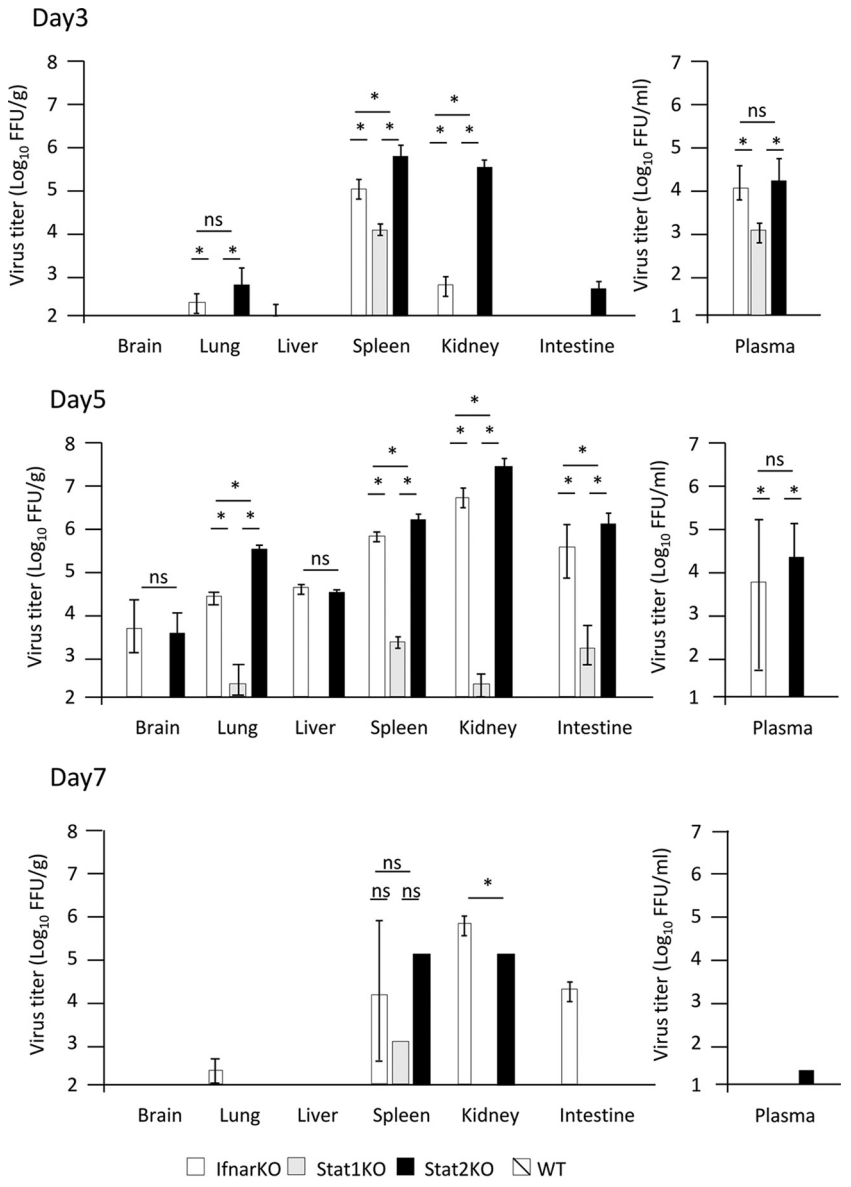

FIG 2 Titers of SFTSV in mouse organs. Mice were inoculated with 10 FFU of SFTSV YG1. Three female mice were euthanized for virus titration at 3, 5, and 7 days p.i. The virus titers in the mouse brains, lungs, livers, spleens, kidneys, intestines, and plasma were measured by focus-forming assay. The values are shown as means ± SDs ($n = 3$). *, $P < 0.05$ for comparisons for each mouse strain.

examined by DLR gene assay. In this experiment, the VP40 protein of mouse-adapted Marburg virus (mMARV), which functions as an IFN signaling inhibitor in murine cells, was used as a positive control (20). As shown in Fig. 3B, IFN-αA/D treatment induced strong ISRE activation in both HEK293T and NIH 3T3 cells. As expected, the expression of SFTSV NSs significantly inhibited the ISRE activation driven by IFN-αA/D in HEK293T cells, while NSs expression did not suppress this activation in NIH 3T3 cells (Fig. 3B). We also confirmed that the ISRE activation driven by IFN-αA/D in NIH 3T3 cells was suppressed by the expression of mMARV VP40 (Fig. 3C). These results suggest that SFTSV NSs cannot interfere with type I IFN signaling in murine cells.

We also examined the effect of NSs on IFN-αA/D-induced expression of mRNA for two ISGs, ISG56 and oligoadenylate synthetase 1 (OAS1), by real-time quantitative PCR (qPCR). The induction of both ISGs by IFN in HEK293T cells was suppressed by NSs expression, whereas NSs did not suppress induction in NIH 3T3 cells (Fig. 3D).

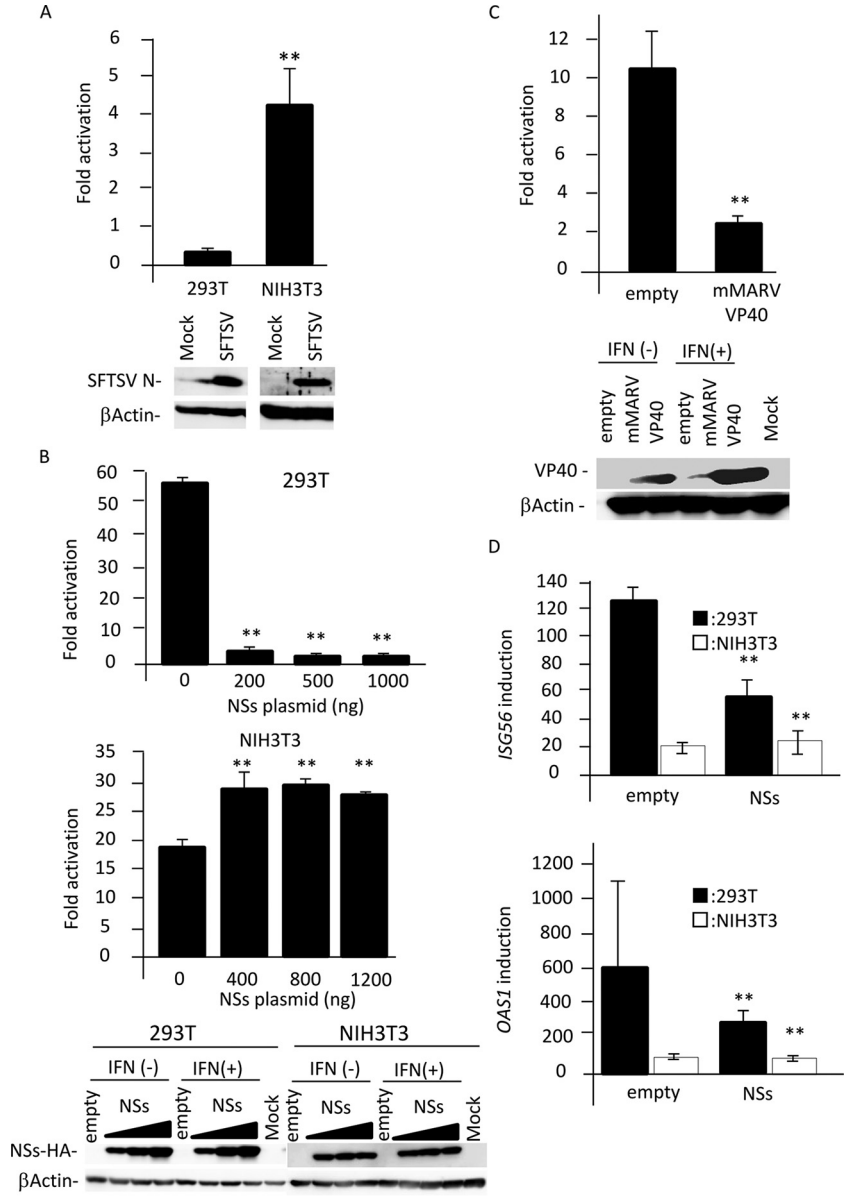

FIG 3 Function of NSs as an IFN antagonist in human and murine cells. (A) HEK293T or NIH 3T3 cells transfected with the reporter plasmids were mock infected or infected with SFTSV. Two days after infection, cells were lysed to measure luciferase activity and to examine protein expression using immunoblotting. Relative light units (RLU) in mock-infected cells were set as 1. Fold activation by SFTSV infection is indicated. (B) The reporter plasmids were transfected into HEK293T or NIH 3T3 cells with or without the expression plasmid for NSs. Twenty-four h after transfection, cells were treated with IFN-αA/D (500 U/ml) or left untreated for 18 h and then were lysed to measure luciferase activity and detect protein expression using immunoblotting. RLU in cells transfected with the empty vector or the indicated amount of NSs expression plasmid in the absence of IFN-αA/D were set as 1. Fold activation by IFN-αA/D is indicated. (C) The experiment depicted in panel B was repeated using the expression plasmid for mMARV VP40 in NIH 3T3 cells. (D) NSs expression plasmid (1 μg or 1.5 μg) or control plasmid was transfected into HEK293T or NIH 3T3 cells, respectively. Twenty-four h after transfection, the cells were treated with IFN-αA/D (200 U/ml) for 10 h or left untreated. Expression levels of *Isg56* and *Oas1* mRNAs in each cell line were measured by real-time qPCR. The mRNA expression levels of ISG56 and OAS1 in untreated cells were set as 1. Fold activation by IFN-αA/D is indicated. These assays were independently performed in triplicate. The data represent averages with SDs. **, $P < 0.05$ versus no NSs.

NSs does not interact with murine and hamster STAT2. SFTSV NSs inhibits type I IFN signaling by the interaction with human STAT1 (hSTAT1) and STAT2 (hSTAT2) (13–15). However, the interaction with hSTAT1 is weaker than that with hSTAT2 (15). We also showed here that mice deficient for STAT2, but not STAT1, were highly susceptible

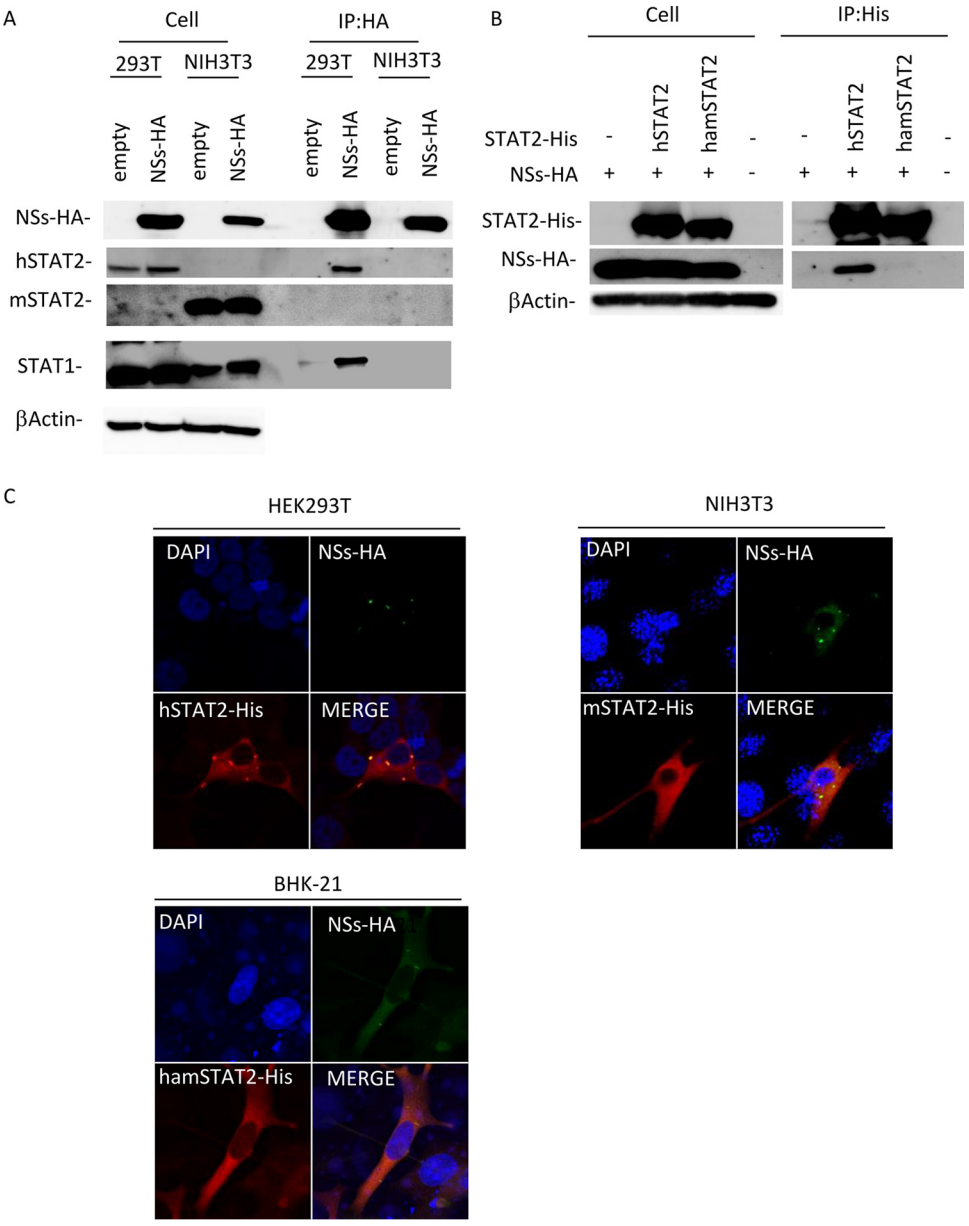

FIG 4 Interaction of NSs with STAT1 and STAT2. (A) HEK293T or NIH 3T3 cells were transfected with the expression plasmid for HA-tagged NSs, and co-IP assays were performed. (B) NIH 3T3 cells were transfected with the expression plasmids for HA-tagged NSs and His-tagged hSTAT2 or hamSTAT2. The protein expression levels in cell lysates (left) and in co-IP assays (right) using an anti-HA or anti-His antibody are shown. (C) Colocalization of NSs with STAT2. HEK293T, NIH 3T3, or BHK-21 cells were transfected with the expression plasmid for HA-tagged NSs and the expression plasmid for His-tagged hSTAT2, mSTAT2, or hamSTAT2, respectively. IFA was also performed with NSs, STAT2, and the nuclei shown in green, red, and blue, respectively.

to SFTSV infection and progressed to severe disease (Fig. 1). Therefore, we suggest that NSs cannot interact with murine STAT2 and, thus, cannot antagonize IFN signaling in murine cells.

First, to examine whether NSs interacts with murine STAT2 (mSTAT2), we performed coimmunoprecipitation (co-IP) assays using lysates from cells transfected with an NSs expression plasmid. As shown in Fig. 4A, co-IP of STAT2 with NSs was observed in the lysates from HEK293T cells but not from NIH 3T3 cells, suggesting that NSs interact with hSTAT2 but not with mSTAT2. It also indicated that NSs bound to hSTAT1 but not to murine STAT1 (mSTAT1) (Fig. 4A).

We also examined the interaction of NSs with hamster STAT2 (hamSTAT2) by co-IP assay, since *Stat2*$^{-/-}$ hamsters, like *Stat2*$^{-/-}$ mice, are highly susceptible to SFTSV infection (19). As shown in Fig. 4B, the interaction of NSs with hamSTAT2, as well as mSTAT2, was not observed.

The interaction of NSs with STAT2 was also examined by subcellular colocalization of the proteins. The NSs expression plasmid was cotransfected with the expression plasmids for hSTAT2, mSTAT2, or hamSTAT2 into HEK293T, NIH 3T3, or BHK-21 cells, respectively, and subcellular localizations of proteins were observed. Cytoplasmic inclusion bodies (IBs), mainly formed by NSs, were also observed in HEK293T, NIH 3T3, and BHK-21 cells (Fig. 4C). In HEK293T cells, hSTAT2 colocalizes with NSs, consistent with previous reports (13–15). On the other hand, in NIH 3T3 and BHK-21 cells, colocalization of NSs with mSTAT2 or hamSTAT2 was not observed (Fig. 4C). These findings indicate that NSs interacts with hSTAT2 but not mSTAT2 and hamSTAT2.

The N-terminal region of hSTAT2 is important for binding to NSs. To investigate the difference in NSs binding between human and murine STAT2, we prepared a series of chimeric proteins from hSTAT2 and mSTAT2 (Fig. 5A). The interactions between NSs and the chimeric STAT2 proteins were examined by co-IP assay. All chimeric proteins were efficiently expressed in NIH 3T3 cells (Fig. 5B). As shown in Fig. 5B, NSs interacted with hSTAT2, HHM, HMM, H(101-315)MM, and H(101-315)HM but not mSTAT2, MHH, MMH, H(1-100)MM, H(1-221)MM, and H(222-315)MM.

We also confirmed the results by observation of colocalization of the proteins (Fig. 5C). NSs colocalized with hSTAT2, HHM, HMM, H(101-315)MM, and H(101-315)HM, while mSTAT2, MHH, MMH, H(1-100)MM, H(1-221)MM, and H(222-315)MM did not colocalize with NSs. These results are consistent with those from the co-IP assay. It has been reported that SFTSV NSs interacts with the DNA-binding domain (DBD; amino acid positions 316 to 485) of hSTAT2 (13). Taken together, these results suggest that region 101-315 of hSTAT2 is important for the binding to NSs in addition to the DBD, or that this region of mSTAT2 interferes with the binding to NSs.

To further examine whether MHH and MMH, which cannot bind to NSs, function as STAT2 proteins in the presence of NSs, ISRE activation by MHH or MMH in the presence of NSs was investigated by the DLR assay in HEK293T cells. ISRE activation was reduced by NSs in the absence of exogenous STAT2, and overexpression of exogenous hSTAT2 slightly compensated for this reduction induced by NSs (Fig. 6). In contrast, the suppression of ISRE activation by NSs was significantly recovered by mSTAT2, MMH, and MHH, suggesting that MMH and MHH, as well as mSTAT2, activate ISRE as a functional STAT2 protein in the presence of NSs in HEK293T cells.

Type I IFN induces the phosphorylation of mSTAT2 in the presence of NSs. Tyrosine phosphorylation of STAT2 is important for its function as a transcription factor in the type I IFN signaling pathway (21). To assess whether type I IFN signaling can phosphorylate mSTAT2 in the presence of NSs, HEK293T and NIH 3T3 cells were transfected with empty vector or the NSs-HA expression plasmid and then treated with IFN-αA/D. The expression levels of hSTAT2 and mSTAT2 were stable regardless of NSs expression (Fig. 7A). In the absence of NSs, IFN induced the phosphorylation of hSTAT2 and mSTAT2. hSTAT2 phosphorylation in HEK293T cells was significantly downregulated by NSs in a concentration-dependent manner. In contrast, mSTAT2 in NIH 3T3 cells was phosphorylated irrespective of NSs expression (Fig. 7A). These were also observed in SFTSV-infected cells (Fig. 7B). It is likely that NSs cannot interfere with the phosphorylation of mSTAT2, since NSs cannot bind to mSTAT2.

DISCUSSION

Previous studies in animal models of SFTSV infection indicated the importance of the type I IFN response in mice and STAT2 in hamsters to prevent disease progression (16, 17, 19). Both STAT1 and STAT2 have been found to be key factors in the IFN signaling pathway (21). In this study, we demonstrated that STAT2-deficient mice, as well as type I IFN receptor-deficient mice, are more susceptible to SFTSV than STAT1-deficient mice and wild-type mice. Moreover, our results indicate that NSs has no ability

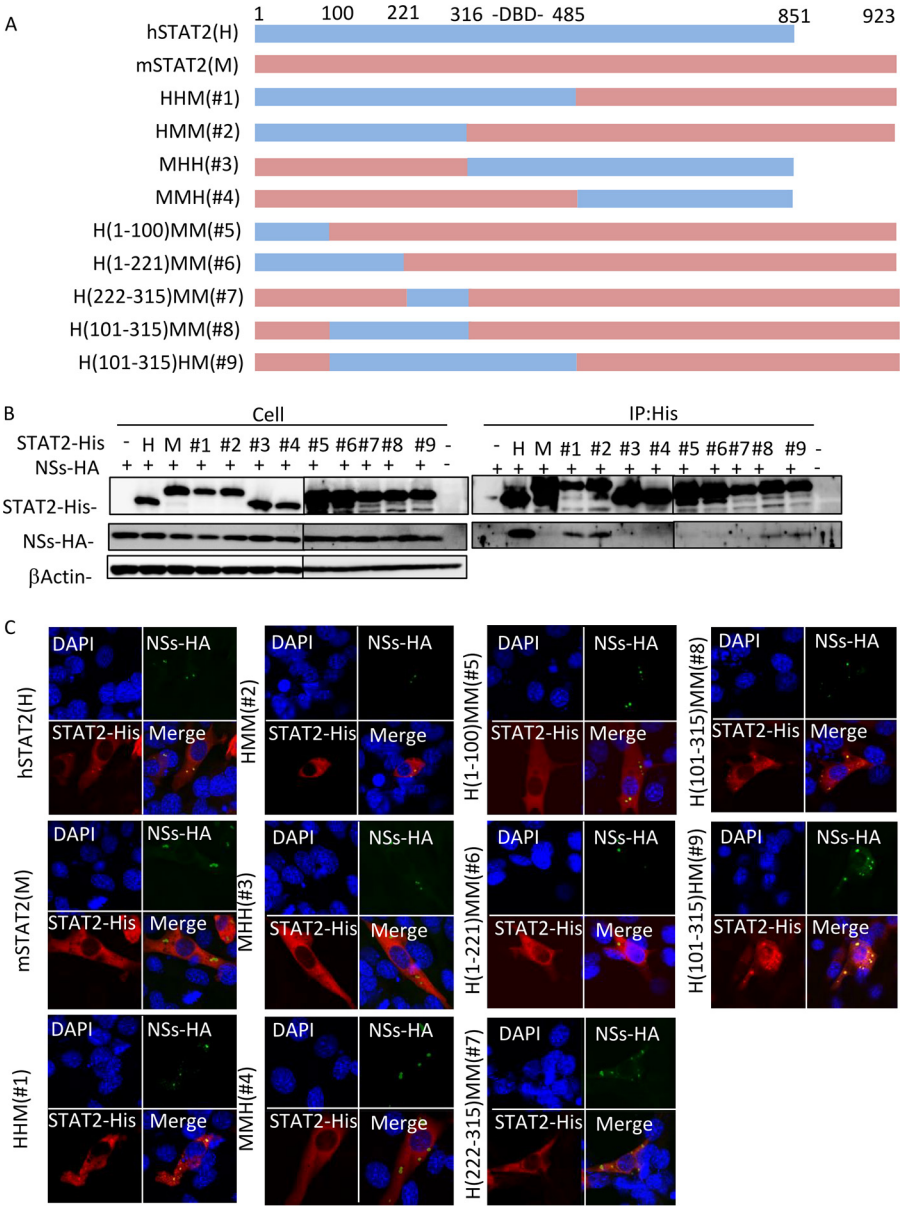

FIG 5 Determination of the region of hSTAT2 important for binding to NSs. (A) Schematic representation of the chimeric mutants of hSTAT2 and mSTAT2. (B) NIH 3T3 cells were cotransfected with the expression plasmids for HA-tagged NSs and each of the STAT2 His-tagged chimeras. Representative results from the protein expression check in cell lysates (upper) and the co-IP assays using an anti-His antibody (lower) are shown. (C) IFA was also performed with NSs, STAT2, and the nuclei shown in green, red, and blue, respectively.

to suppress the IFN signaling pathway in murine cells because NSs, which binds hSTAT1 and hSTAT2, cannot interact with mSTAT1 and mSTAT2. SFTSV growth in the organs of *Stat1*$^{-/-}$ mice was much less efficient than that in *Stat2*$^{-/-}$ and *Ifnar1*$^{-/-}$ mice, although SFTSV could grow in *Stat1*$^{-/-}$ mice (Fig. 2). In addition, SFTSV infection induced milder symptoms in *Stat1*$^{-/-}$ mice than in *Stat2*$^{-/-}$ and *Ifnar1*$^{-/-}$ mice (Fig. 1). These findings suggest that innate immunity dependent on STAT2, but not STAT1, strongly inhibits the replication of SFTSV in mice. In several human cell lines, the expression of some ISGs is upregulated by STAT2 independent of STAT1 (22). For example, the expression levels of several ISGs, including APOBEC3G, PKR, ISG15, and Mx1, are increased by type I IFN stimulation regardless of STAT1 expression in the human liver cell lines Huh7 and Hep3B. However, when the expression of STAT2 is

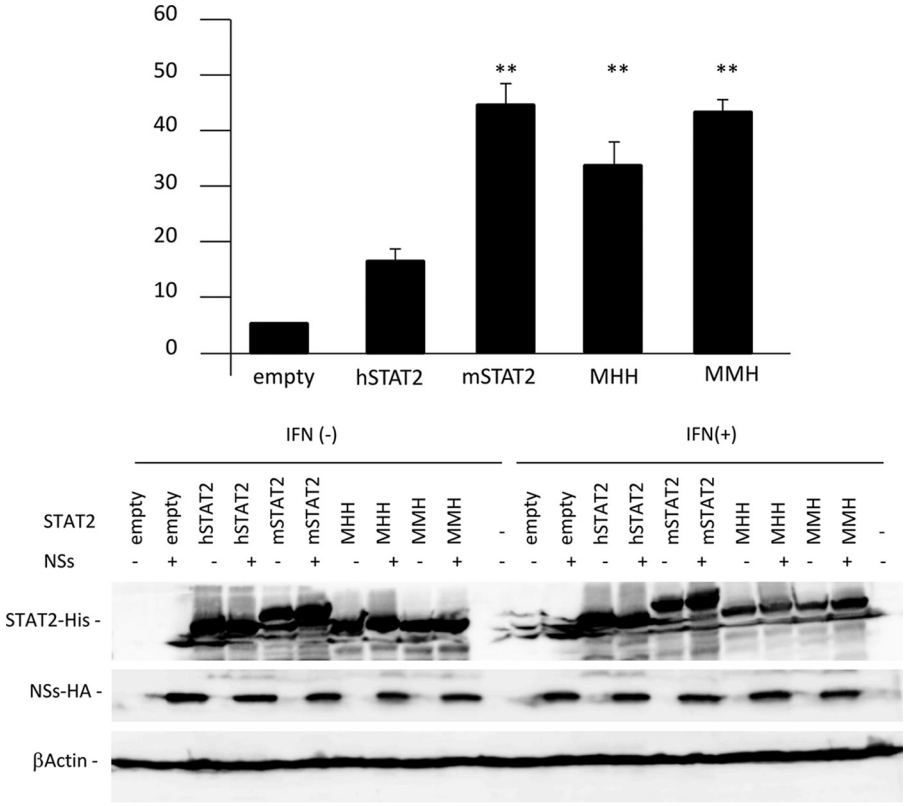

FIG 6 Function of the NSs binding-deficient STAT2 chimera. The reporter plasmids were cotransfected into HEK293T cells with the expression plasmids for NSs and each STAT2 chimera. Twenty-four h after transfection, cells were treated with IFN-αA/D (500 U/ml) for 18 h or left untreated and then were lysed to measure luciferase activity (upper) or detect protein expression using immunoblotting (lower). The ISRE activity was calculated by dividing RLU in IFN-αA/D-treated cells by the units of cells not treated with IFN-αA/D. The ISRE activity in the absence of NSs was set as 100%. The assays were independently performed in triplicate. The data represent averages with SDs. **, $P < 0.05$ versus hSTAT2.

suppressed, the expression levels of these ISGs are not increased after type I IFN treatment. These findings suggest that ISG expression mediated by STAT2, but not STAT1, mainly suppresses SFTSV infection in mice.

SFTSV causes severe disease in humans, while immunocompetent adult mice never show any apparent severe symptoms after SFTSV infection (18). In this study, we showed that mice lacking STAT2 are highly susceptible to SFTSV infection. Moreover, NSs can suppress the phosphorylation of hSTAT2, whereas the phosphorylation of mSTAT2 is not inhibited by NSs due to the inability of NSs to bind to mSTAT2. The data also indicate that NSs cannot interact with hamSTAT2. This result is consistent with a previous report that showed that STAT2-deficient hamsters are also highly susceptible to SFTSV infection (19).

The relationship between NSs and STAT2 is reminiscent of that of dengue virus NS5 and STAT2 (23–25). Previous studies reported that innate immunity mediated by mSTAT2 restricts dengue virus replication in mice (25, 26). To block the type I IFN signaling pathway in humans, dengue virus NS5 expression leads to the degradation of hSTAT2 (25). However, NS5 cannot suppress type I IFN signaling in mice, because mSTAT2 is resistant to NS5-mediated degradation (23–25). These results demonstrate that STAT2 may be one of the determinants for the species specificity of dengue virus. Here, we elucidated that SFTSV induces lethal disease in STAT2-deficient mice and that NSs cannot interact with mSTAT2. Thus, similar to dengue virus NS5, the anti-STAT2 activity of NSs appears to determine the species specificity of SFTSV infection.

In this study, chimeric mutants of hSTAT2 and mSTAT2 revealed that residues 101 to 315 of hSTAT2 are required for the interaction with NSs or that these residues in

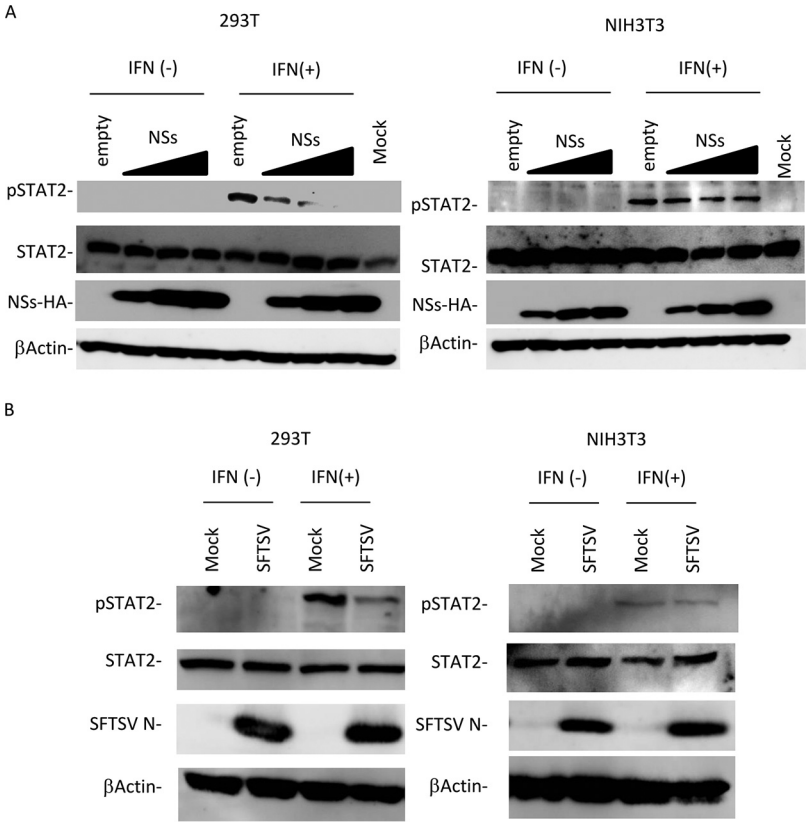

FIG 7 Suppression of STAT2 phosphorylation by NSs. (A) HEK293T or NIH 3T3 cells transfected with the expression plasmid for HA-tagged NSs were treated with IFN-αA/D (2,000 U/ml) for 45 min or left untreated and were then lysed for detection of expression of each protein by immunoblotting. (B) HEK293T or NIH 3T3 cells infected with SFTSV at an MOI of 10 were treated with IFN-αA/D (2,000 U/ml) for 45 min or left untreated and were then lysed for detection of expression of each protein by immunoblotting.

mSTAT2 interfere with the interaction with NSs. We also confirmed that mSTAT2 and all of the chimeric mutants of hSTAT2 and mSTAT2 used in this study can activate ISRE-mediated gene expression as functional STAT2 proteins. Previously, Ning et al. reported that the DBD region (316-485) of hSTAT2 is required for the interaction with NSs (13). However, we showed that mutants possessing the DBD region of mSTAT2, HMM, and H(101-315)MM can still bind to NSs (Fig. 5). At present, we cannot explain this result, although this discrepancy may be explained by the differences in the three-dimensional protein structure between our mutants and Ning et al.'s deletion mutants. Further analyses will be required to clarify this issue.

Taken together, we conclude that the anti-STAT2 activity of NSs determines the species specificity of SFTSV infection. In addition, we show that *Stat2*$^{-/-}$ mice, as well as *Ifnar1*$^{-/-}$ mice and *Stat2*$^{-/-}$ hamsters, are highly susceptible to SFTSV infection, which causes lethal disease, suggesting that *Stat2*$^{-/-}$ mice are useful as an animal model to develop antiviral drugs against SFTSV infection.

MATERIALS AND METHODS

Ethics statement. Our research protocol for the use of mice follows the Nagasaki University Regulations for Animal Care and Use, which were approved by the Animal Experiment Committee of Nagasaki University (approval number 151110-1-5).

Animals. The B6.129-Dnase2a<tm10sa>Ifnar1<tm1Agt> mouse strain (RBRC04021; *Ifnar1*$^{-/-}$ *Dnase2a*$^{+/-}$) (27) was provided by RIKEN BRC through the National BioResource Project of MEXT, Japan. *Ifnar1*$^{-/-}$ mice were generated by crossing *Dnase2a*$^{+/-}$ *Ifnar1*$^{-/-}$ parents. *Stat1*$^{-/-}$ mice were provided by Takayuki Yoshimoto (Tokyo Medical University). *Stat2*$^{-/-}$ mice were purchased from the Jackson Laboratory. The genetic background of all mice used in this study is C57BL/6.

SFTSV infection in mice. Six- to 8-week-old male or female mice were used in this study. In infection experiments, each mouse was infected with SFTSV by intradermal injection (50 μl of virus solution for 10 FFU). Mouse survival and body weight changes were monitored daily for 14 days p.i. At 1, 3, and 7 days p.i., blood was collected and platelets and leukocytes were counted using a hematology analyzer (Sysmex pocH-100iV; Sysmex or VetScan HMII; Abaxis). Mice were euthanized, and plasma and organs (lungs, livers, spleens, kidneys, intestines, and brains) were collected. Viruses in plasma were titrated by focus-forming assay using Vero E6 cells. To determine the titer of SFTSV in organs, mouse organs were collected in a 9-fold volume of minimum essential medium (Sigma-Aldrich) and then disrupted through high-speed shaking using a TissueLyser II (Qiagen). After centrifugation (700 $\times$ *g*, 5 min, 4°C), the amounts of viruses in the homogenates (10%, wt/vol) were determined by focus-forming assay in Vero E6 cells. The limit of detection was 100 FFU/g.

Cell culture and virus. Human embryonic kidney (HEK) 293T (CRL-11268; ATCC), NIH 3T3 (CRL-1658; ATCC), BHK-21 (JCRB9020; Health Science Research Resources Bank [HSRRB]), and Vero E6 (CRL-1586; ATCC) cells were cultured in Dulbecco's modified Eagle's medium (Sigma-Aldrich) supplemented with 10% heat-inactivated fetal calf serum (FCS) and antibiotics (Thermo Fisher Scientific). SFTSV YG-1, a field isolate from an SFTS patient in Japan, was kindly provided by Ken Maeda, Yamaguchi University (4). The virus stocks were prepared from culture supernatants of Vero E6 cells.

Focus-forming assay. SFTSV titers were determined using a focus-forming assay. Briefly, confluent monolayers of Vero E6 cells were inoculated with 10-fold dilutions of SFTSV and incubated at 37°C for 1 h. The inoculum was removed, and cells were washed and overlaid with minimal essential medium (Sigma-Aldrich) containing 0.7% agarose and 0.7% FCS. After 4 days, cells were fixed with 4% paraformaldehyde and permeabilized with phosphate-buffered saline (PBS) containing 1% Triton X-100. Cells were blocked with PBS containing 0.1% Triton X-100 and 1% bovine serum albumin (BSA) and then incubated with anti-SFTSV N protein rabbit polyclonal antibody (28). After washing with PBS, the cells were incubated with anti-rabbit IgG conjugated with horseradish peroxidase (HRP; Promega). After more washes with PBS, SFTSV-infected cells were detected by using the peroxidase stain DAB kit and metal enhancer for DAB stain (Nacalai Tesque). The number of SFTSV N-positive cells was determined and normalized as FFU per milliliter.

Plasmids. The open reading frame (ORF) encoding NSs was amplified by reverse transcription-PCR (RT-PCR) from SFTSV (YG-1) viral RNA and inserted into pcDNA3.1 (Invitrogen) with a hemagglutinin (HA) tag using the primers listed in Table 1 to produce pcDNA3.1/NSs-HA. To prepare the expression plasmids for 6$\times$ histidine (6$\times$His)-tagged hSTAT2 (pcDNA3.1/hSTAT2-His), mSTAT2 (pcDNA3.1/mSTAT2-His), and hamSTAT2 (pcDNA3.1/hamSTAT2-His), the desired genes were amplified by RT-PCR using the primers listed in Table 1 from the cDNA of HEK293T, NIH 3T3, and BHK-21 cells, respectively. The expression plasmids for the series of STAT2 chimeras were constructed using an In-Fusion HD cloning kit (TaKaRa) with the primers listed in Table 1. The expression plasmid for mMARV VP40 was constructed from MARV VP40 (29) using a KOD-Plus mutagenesis kit (Toyobo) using the primers listed in Table 1.

Reporter gene assay. HEK293T cells and NIH 3T3 cells were cotransfected with ISRE reporter plasmid (450 ng) (Promega) and pRL-TK plasmid (the *Renilla* luciferase control plasmid for the constitutively active herpes simplex virus [HSV]-thymidine kinase [TK] promoter) (100 ng) (Promega). Twenty-four h after transfection, the transfected cells were mock infected or infected with SFTSV. Two days after infection, luciferase activities were measured with a DLR assay kit (Promega) and a TriStar LB941 system (Berthold).

For the reporter gene assays with SFTSV NSs transfection, the ISRE reporter plasmid (500 ng) (Promega) and pRL-TK plasmid (100 ng) (Promega) were transfected into HEK293T and NIH 3T3 cells with or without the indicated amount of pcDNA3.1/NSs-HA plasmid or the expression plasmid for mMARV VP40 (800 ng) using LT-1 (Mirus) or Lipofectamine 3000 (Thermo Fisher Scientific) according to the manufacturer's instructions. Twenty-four h after transfection, cells were treated with IFN-αA/D (500 U/ml) (Sigma-Aldrich) or were left untreated for 18 h. Luciferase activities then were measured with a DLR assay kit (Promega) and a TriStar LB941 system (Berthold).

Quantitative RT-PCR of IFN-treated cells. Total RNA was extracted from HEK293T and NIH 3T3 cells using an RNeasy Minikit (Qiagen). Real-time RT-PCR was performed by using the one-step TB Green PrimeScript Plus RT-PCR kit (TaKaRa) according to the manufacturer's instructions, and the PCR primers used in this study are listed in Table 1. Relative mRNA levels were calculated by the $2^{-\Delta\Delta CT}$ method with glyceraldehyde-3-phosphate dehydrogenase (*GAPDH*) mRNA as an internal control and are shown as relative fold changes normalized to the untreated control samples.

Immunoblotting. Protein samples were separated by SDS-PAGE and transferred to nitrocellulose membranes (Millipore). After blocking with 5% skim milk in Tris-buffered saline–Tween 20 (TBS-T), the membranes were incubated with each of the following antibodies: anti-HA (18850; QED Biosciences Inc.), anti-His (9F2; Wako), anti-hSTAT2 (A-9; Santa Cruz), anti-mSTAT2 (07-140; Merck), anti-STAT2 (phosphor Y690; ab53132; Abcam), anti-STAT1 (D19KY; Cell Signaling), and anti-β actin (AC-15; Sigma-Aldrich). After washing with TBS-T, the membranes were incubated with horseradish peroxidase-labeled secondary antibodies, anti-mouse IgG-HRP (A2304; Sigma-Aldrich), or anti-rabbit IgG-HRP (WA4011; Promega) and then detected using ECL prime (GE Healthcare) according to the manufacturer's instructions. Bands were visualized using an image analyzer (LAS-4000 mini; GE Healthcare).

Co-IP assay. To examine the binding of NSs to endogenous STAT2, the pcDNA3.1/NSs-HA plasmid (15 μg) was transfected into HEK293T and NIH 3T3 cells in 10-cm dishes (Thermo Fisher Scientific) using LT-1 or Lipofectamine 3000, respectively. To examine the binding of NSs to exogenous STAT2 or STAT2 derivatives, the pcDNA3.1/NSs-HA plasmid (3 μg) was cotransfected into NIH 3T3 cells with each STAT2 expression plasmid (1 μg) in 6-well plates (Thermo Fisher Scientific) using Lipofectamine 3000. Two days after transfection, cells were lysed in lysis buffer (25 mM Tris-HCl, 150 mM NaCl, 1 mM EDTA, and 1%

TABLE 1 List of the primers used in this study

Name	Sequence	Remark[a]
pcDNA-NSsHA-RV-F	ATCCACCATGTCGCTGAGCAAATGCTCCAAC	For construction of pcDNA3.1/NSs-HA
pcDNA-NSsHA-Kpn-R	GCTTGGTACCTCAAGCGTAATCTGGAACATCGTATGGATAGAC CTCCTTCGGGAGGTCACC	
humanSTAT2hisF	ATCCACCATGGCGCAGTGGGAAATGCTG	For construction of pcDNA3.1/hSTAT2-His
humanSTAT2hisR	GCTTGGTACCTCAATGGTGATGGTGATGATGACCGGTATGCATATTGAAGT CAGAAGGCATCAAGGGTCC	
mouseSTAT2hisF	ATCCACCATGGCGCAGTGGGAGATGTTG	For construction of pcDNA3.1/mSTAT2-His
mouseSTAT2hisR	GCTTGGTACCTCAATGGTGATGGTGATGATGACCGGTATGCATATTGAAG GTATCAAGAGTCCATCCCAA	
hamSTAT2F	ATCCACCATGGCGCAGTGGGAGACACTG	For construction of pcDNA3.1/hamSTAT2-His
hamSTAT2hisR	GCTTGGTACCTCAATGGTGATGGTGATGATGACCGGTATGCATATTGTCAT CAGAAGGAATCAAGGGTCC	
mSTAT2-hDBD-veF	GTTCTTCTGCCAAGCTCCGAAAG	For construction of pHHM(#1)
HMM-HHM-inR	ACCGGTATGCATATTGAAGGTATC	
hmSTAT2DBDveF	AATATGCATACCGGTCATCATCAC	
mSTAT2-hDBD-inR	GCTTGGCAGAAGAACTGCTGGTTCTGAAGG	
hSTAT2-mDBD-inF	ACAGAGCCTTTGTAGTAGAAACCCAGCCCTG	For construction of pHMM(#2)
HMM-HHM-inR	ACCGGTATGCATATTGAAGGTATC	
hmSTAT2DBDveF	AATATGCATACCGGTCATCATCAC	
hSTAT2-mDBD-veR	CTACAAAGGCTCTGTGGAGCAG	
mSTAT2-hDBD-inF	AAAGGTCCTTTGTGGTAGAAACCCAGCCC	For construction of pMHH(#3)
MMH-MHH-inR	ACCGGTATGCATATTGAAGTCAG	
hmSTAT2DBDveF	AATATGCATACCGGTCATCATCAC	
mSTAT2-hDBD-veR	CCACAAAGGACCTTTGGAGCAGAC	
hSTAT2-mDBD-veF	GTTCTTCTCCAACCCCCCCAAG	For construction of pMMH(#4)
MMH-MHH-inR	ACCGGTATGCATATTGAAGTCAG	
hmSTAT2DBDveF	AATATGCATACCGGTCATCATCAC	
hSTAT2-mDBD-inR	GGGTTGGAGAAGAACTGCTGGTTCTTGGG	
H(1-100)MminF	CCCAGGATCCTACCCAGTTGGCTGAGATG	For construction of pH(1-100)MM(#5)
HMM-HHM-inR	ACCGGTATGCATATTGAAGGTATC	
hmSTAT2DBDveF	AATATGCATACCGGTCATCATCAC	
H(1-100)MMVeR	GGGTAGGATCCTGGGAAAAGGGCTGAATG	
H(1-221)MminF	CACTGCTAGGCCGATTAACCACCCTGG	For construction of pH(1-221)MM(#6)
HMM-HHM-inR	ACCGGTATGCATATTGAAGGTATC	
hmSTAT2DBDveF	AATATGCATACCGGTCATCATCAC	
H(1-221)MMVeR	ATCGGCCTAGCAGTGCTTTGGAGGCATC	
H222-315inF	GACTGGTTGGCCGATTAACTACCCTAATCG	For construction of pH(222-315)MM(#7)
hSTAT2-mDBD-veR	CTACAAAGGCTCTGTGGAGCAG	
hSTAT2-mDBD-inF	ACAGAGCCTTTGTAGTAGAAACCCAGCCCTG	
H222-315veR	ATCGGCCAACCAGTCCTTTGGAGATGTCC	
MH(101-315)MminF	CCCAATGGCCCTACCCAGTTGGCTGAGATG	For construction of pH(101-315)MM(#8)
hSTAT2-mDBD-veR	CTACAAAGGCTCTGTGGAGCAG	
hSTAT2-mDBD-inF	ACAGAGCCTTTGTAGTAGAAACCCAGCCCTG	
MH(101-315)MMveR	GGTAGGGCCATTGGGAAAGGTCTGAATATC	
MH(101-315)MminF	CCCAATGGCCCTACCCAGTTGGCTGAGATG	For construction of pH(101-315)HM(#9)
HMM-HHM-inR	ACCGGTATGCATATTGAAGGTATC	
hmSTAT2DBDveF	AATATGCATACCGGTCATCATCAC	
MH(101-315)MMveR	GGTAGGGCCATTGGGAAAGGTCTGAATATC	
MARV VP40 S15PF	CTTGAACCCCCCTCCTTATGCTGATCACGG	For construction of pmMARV VP40
MARV VP40 S15PR	TATTGCATGTATGTGTTGTAATTGCTGGAACTGGCC	
MARV VP40 G79SF	GTTCCGGCATGGCTGCCTCTTGG	
MARV VP40 G79SR	GCTTTTGACTGTTCGCTCGTTATATGCAGATATGTC	
hISG56F	CCTCCTTGGGTTCGTCTACA	For real-time RT-PCR detection of human ISG56 (Ref. 13)
hISG56R	GGCTGATATCTGGGTGCCTA	

(Continued on next page)

TABLE 1 (Continued)

Name	Sequence	Remark[a]
mISG56F mISG56R	ACCATGGGAGAGAATGCTGAT GCCAGAGGTTGTGC	For real-time RT-PCR detection of mouse ISG56 (Ref. 30)
hOAS1realF hOAS1realR	CATCCGCCTAGTCAAGCACTG CACCACCCAAGTTTCCTGTAG	For real-time RT-PCR detection of human OAS1 (Ref. 13)
mOAS1realF mOAS1realR	GCCTGGTCACGCACTGGTA AAGCCCTGGGCTGTGTTG	For real-time RT-PCR detection of mouse OAS1 (Ref. 31)
hGAPDH-F hGAPDH-R	ATGGGGAAGGTGAAGGTCGG TTACTCCTTGGAGGCCATGTG	For real-time RT-PCR detection of human GAPDH
mGAPDH-F mGAPDH-R	AGGTCGGTGTGAACGGATTTG TGTAGACCATGTAGTTGAGGTCA	For real-time RT-PCR detection of mouse GAPDH (Ref. 32)

[a]Ref., reference.

Triton X-100) containing a protease inhibitor cocktail (Roche). To perform the co-IP assay, cell lysates were mixed with magnetic beads conjugated to an anti-His monoclonal antibody (OGHis; MBL) or anti-HA monoclonal antibody (5D8; MBL) and incubated at 4°C for 3 h or overnight, respectively. The magnetic beads then were washed with lysis buffer and wash buffer (50 mM Tris-HCl, 1% NP-40, 0.25% deoxycholic acid sodium salt, 150 mM NaCl, and 1 mM EDTA) and analyzed by immunoblotting as described above.

Immunofluorescence assay (IFA). The expression plasmids for His-tagged hSTAT2, mSTAT2, hamSTAT2, or a series of STAT2 chimeras were cotransfected into HEK293T, NIH 3T3, or BHK-21 cells with the pcDNA3.1/NSs-HA plasmid. Twenty-four h after transfection, transfected cells were fixed using 4% paraformaldehyde–PBS (Wako), and then the fixed cells were incubated in 1% Triton X-100 in PBS for permeabilization and blocked in 10% FCS in blocking buffer (3% BSA and 0.3% Triton X-100 in PBS). Cells then were treated with primary antibodies (anti-HA [18850; QED Biosciences Inc.] or anti-His [9F2; Wako]) overnight at 4°C and stained with secondary antibodies (anti-rabbit IgG-H&L [fluorescein isothiocyanate] [ab6009; Abcam] or anti-mouse IgG [whole molecule]-tetramethyl rhodamine isothiocyanate [T5393; Sigma-Aldrich]) for 2 h at room temperature with 4′,6-diamidino-2-phenylindole (Roche) for visualization of nuclei. Image acquisition was performed with an LSM780 microscope (Carl Zeiss).

Statistical analyses. Significant differences in virus titers in mouse organs among mouse strains were determined by one-way analysis of variance following Tukey's multiple-comparison test using GraphPad Prism software. Statistically significant differences in the data of Fig. 3A to D and 6 were determined using Student's *t* test (Fig. 3A, C, and D) or Dunnett's test (Fig. 3B and 6).

ACKNOWLEDGMENTS

We thank K. Maeda (Yamaguchi University, Yamaguchi, Japan) and T. Yoshimoto (Tokyo Medical University, Tokyo, Japan) for providing the SFTSV YG1 strain and *Stat1*$^{-/-}$ mice, respectively. We also thank S. Morikawa and S. Fukushi (National Institute of Infectious Diseases, Tokyo, Japan) for providing the anti-SFTSV N antibody. We are grateful to all the members of the Department of Emerging Infectious Diseases, Institute of Tropical Medicine, Nagasaki University.

This research was supported by a grant from the Japan Agency for Medical Research and Development (AMED) under grant number JP18fk0108202 (J.Y.), the Japan Society for the Promotion of Science under grant number 15J06242 (R.Y.), and the Takeda Science Foundation (R.Y.).

REFERENCES

1. Yu XJ, Liang MF, Zhang SY, Liu Y, Li JD, Sun YL, Zhang L, Zhang QF, Popov VL, Li C, Qu J, Li Q, Zhang YP, Hai R, Wu W, Wang Q, Zhan FX, Wang XJ, Kan B, Wang SW, Wan KL, Jing HQ, Lu JX, Yin WW, Zhou H, Guan XH, Liu JF, Bi ZQ, Liu GH, Ren J, Wang H, Zhao Z, Song JD, He JR, Wan T, Zhang JS, Fu XP, Sun LN, Dong XP, Feng ZJ, Yang WZ, Hong T, Zhang Y, Walker DH, Wang Y, Li DX. 2011. Fever with thrombocytopenia associated with a novel bunyavirus in China. N Engl J Med 364:1523–1532. https://doi.org/10.1056/NEJMoa1010095.
2. Denic S, Janbeih J, Nair S, Conca W, Tariq WU, Al-Salam S. 2011. Acute thrombocytopenia, leucopenia, and multiorgan dysfunction: the first case of SFTS bunyavirus outside China? Case Rep Infect Dis 2011:204056.
3. Kim KH, Yi J, Kim G, Choi SJ, Jun KI, Kim NH, Choe PG, Kim NJ, Lee JK, Oh MD. 2013. Severe fever with thrombocytopenia syndrome, South Korea, 2012. Emerg Infect Dis 19:1892–1894.
4. Takahashi T, Maeda K, Suzuki T, Ishido A, Shigeoka T, Tominaga T, Kamei T, Honda M, Ninomiya D, Sakai T, Senba T, Kaneyuki S, Sakaguchi S, Satoh A, Hosokawa T, Kawabe Y, Kurihara S, Izumikawa K, Kohno S, Azuma T, Suemori K, Yasukawa M, Mizutani T, Omatsu T, Katayama Y, Miyahara M, Ijuin M, Doi K, Okuda M, Umeki K, Saito T, Fukushima K, Nakajima K, Yoshikawa T, Tani H, Fukushi S, Fukuma A, Ogata M, Shimojima M, Nakajima N, Nagata N, Katano H, Fukumoto H, Sato Y, Hasegawa H, Yamagishi T, Oishi K, Kurane I, Morikawa S, Saijo M. 2014.

The first identification and retrospective study of severe fever with thrombocytopenia syndrome in Japan. J Infect Dis 209:816–827. https://doi.org/10.1093/infdis/jit603.
5. McMullan LK, Folk SM, Kelly AJ, MacNeil A, Goldsmith CS, Metcalfe MG, Batten BC, Albarino CG, Zaki SR, Rollin PE, Nicholson WL, Nichol ST. 2012. A new phlebovirus associated with severe febrile illness in Missouri. N Engl J Med 367:834–841. https://doi.org/10.1056/NEJMoa1203378.
6. Cui N, Bao XL, Yang ZD, Lu QB, Hu CY, Wang LY, Wang BJ, Wang HY, Liu K, Yuan C, Fan XJ, Wang Z, Zhang L, Zhang XA, Hu LP, Liu W, Cao WC. 2014. Clinical progression and predictors of death in patients with severe fever with thrombocytopenia syndrome in China. J Clin Virol 59:12–17. https://doi.org/10.1016/j.jcv.2013.10.024.
7. Lu QB, Yang ZD, Wang LY, Qin SL, Cui N, Wang HY, Li H, Liu K, Hu JG, Zhang XA, Liu W, Cao WC. 2015. Discrimination of novel bunyavirus infection using routine laboratory test. Clin Microbiol Infect 204: e1–e7.
8. Cui N, Liu R, Lu QB, Wang LY, Qin SL, Yang ZD, Zhuang L, Liu K, Li H, Zhang XA, Hu JG, Wang JY, Liu W, Cao WC. 2015. Severe fever with thrombocytopenia syndrome bunyavirus-related human encephalitis. J Infect 70:52–59. https://doi.org/10.1016/j.jinf.2014.08.001.
9. Koyama S, Ishii KJ, Coban C, Akira S. 2008. Innate immune response to viral infection. Cytokine 43:336–341. https://doi.org/10.1016/j.cyto.2008.07.009.
10. Habjan M, Pichlmair A. 2015. Cytoplasmic sensing of viral nucleic acids. Curr Opin Virol 11:31–37. https://doi.org/10.1016/j.coviro.2015.01.012.
11. Schneider WM, Chevillotte MD, Rice CM. 2014. Interferon-stimulated genes: a complex web of host defenses. Annu Rev Immunol 32:513–545. https://doi.org/10.1146/annurev-immunol-032713-120231.
12. Wuerth JD, Weber F. 2016. Phleboviruses and the type I interferon response. Viruses 8:174. https://doi.org/10.3390/v8060174.
13. Ning YJ, Feng K, Min YQ, Cao WC, Wang M, Deng F, Hu Z, Wang H. 2015. Disruption of type I interferon signaling by the nonstructural protein of severe fever with thrombocytopenia syndrome virus via the hijacking of STAT2 and STAT1 into inclusion bodies. J Virol 89:4227–4236. https://doi.org/10.1128/JVI.00154-15.
14. Chaudhary V, Zhang S, Yuen KS, Li C, Lui PY, Fung SY, Wang PH, Chan CP, Li D, Kok KH, Liang M, Jin DY. 2015. Suppression of type I and type III IFN signalling by NS of severe fever with thrombocytopenia syndrome virus through inhibition of STAT1 phosphorylation and activation. J Gen Virol 96:3204–3211. https://doi.org/10.1099/jgv.0.000280.
15. Rezelj VV, Li P, Chaudhary V, Elliott RM, Jin DY, Brennan B. 2017. Differential antagonism of human innate immune responses by tick-borne phlebovirus nonstructural proteins. mSphere 28:e00234-17.
16. Tani H, Fukuma A, Fukushi S, Taniguchi S, Yoshikawa T, Iwata-Yoshikawa N, Sato Y, Suzuki T, Nagata N, Hasegawa H, Kawai Y, Uda A, Morikawa S, Shimojima M, Watanabe H, Saijo M. 2016. Efficacy of T-705 (favipiravir) in the treatment of infections with lethal severe fever with thrombocytopenia syndrome virus. mSphere 1:e00061-15.
17. Liu Y, Wu B, Paessler S, Walker DH, Tesh RB, Yu XJ. 2014. The pathogenesis of severe fever with thrombocytopenia syndrome virus infection in alpha/beta interferon knockout mice: insights into the pathologic mechanisms of a new viral hemorrhagic fever. J Virol 88:1781–1786. https://doi.org/10.1128/JVI.02277-13.
18. Jin C, Liang M, Ning J, Gu W, Jiang H, Wu W, Zhang F, Li C, Zhang Q, Zhu H, Chen T, Han Y, Zhang W, Zhang S, Wang Q, Sun L, Liu Q, Li J, Wang T, Wei Q, Wang S, Deng Y, Qin C, Li D. 2012. Pathogenesis of emerging severe fever with thrombocytopenia syndrome virus in C57/BL6 mouse model. Proc Natl Acad Sci U S A 109:10053–10058. https://doi.org/10.1073/pnas.1120246109.
19. Gowen BB, Westover JB, Miao J, Van Wettere AJ, Rigas JD, Hickerson BT, Jung KH, Li R, Conrad BL, Nielson S, Furuta Y, Wang Z. 2017. Modeling severe fever with thrombocytopenia syndrome virus infection in golden Syrian hamsters: importance of STAT2 in preventing disease and effective treatment with favipiravir. J Virol 91:e01942-16.
20. Feagins AR, Basler CF. 2015. Amino acid residue at position 79 of Marburg virus VP40 confers interferon antagonism in mouse cells. J Infect Dis 2:219–225.
21. Ivashkiv LB, Donlin LT. 2014. Regulation of type I interferon responses. Nat Rev Immunol 14:36–49. https://doi.org/10.1038/nri3581.
22. Sarkis PT, Ying S, Xu R, Yu XF. 2006. STAT1-independent cell type-specific regulation of antiviral APOBEC3G by IFN-alpha. J Immunol 177: 4530–4540. https://doi.org/10.4049/jimmunol.177.7.4530.
23. Ashour J, Laurent-Rolle M, Shi P-Y, García-Sastre A. 2009. NS5 of dengue virus mediates STAT2 binding and degradation. J Virol 83:5408–5418. https://doi.org/10.1128/JVI.02188-08.
24. Mazzon M, Jones M, Davidson A, Chain B, Jacobs M. 2009. Dengue virus NS5 inhibits interferon-alpha signaling by blocking signal transducer and activator of transcription 2 phosphorylation. J Infect Dis 200: 1261–1270. https://doi.org/10.1086/605847.
25. Ashour J, Morrison J, Laurent-Rolle M, Belicha-Villanueva A, Plumlee CR, Bernal-Rubio D, Williams KL, Harris E, Fernandez-Sesma A, Schindler C, García-Sastre A. 2010. Mouse STAT2 restricts early dengue virus replication. Cell Host Microbe 18:410–421. https://doi.org/10.1016/j.chom.2010.10.007.
26. Perry ST, Buck MD, Lada SM, Schindler C, Shresta S. 2011. STAT2 mediates innate immunity to Dengue virus in the absence of STAT1 via the type I interferon receptor. PLoS Pathog 7:e1001297. https://doi.org/10.1371/journal.ppat.1001297.
27. Yoshida H, Okabe Y, Kawane K, Fukuyama H, Nagata S. 2005. Lethal anemia caused by interferon-beta produced in mouse embryos carrying undigested DNA. Nat Immunol 6:49–56. https://doi.org/10.1038/ni1146.
28. Urata S, Uno Y, Kurosaki Y, Yasuda J. 2018. The cholesterol, fatty acid and triglyceride synthesis pathways regulated by site 1 protease (S1P) are required for efficient replication of severe fever with thrombocytopenia syndrome virus. Biochem Biophys Res Commun 503:631–636. https://doi.org/10.1016/j.bbrc.2018.06.053.
29. Urata S, Noda T, Kawaoka Y, Morikawa S, Yokosawa H, Yasuda J. 2007. Interaction of Tsg101 with Marburg virus VP40 depends on the PPPY motif, but not the PT/SAP motif as in the case of Ebola virus, and Tsg101 plays a critical role in the budding of Marburg virus-like particles induced by VP40, NP, and GP. J Virol 81:4895–4899. https://doi.org/10.1128/JVI.02829-06.
30. Lee KG, Kim SS, Kui L, Voon DC, Mauduit M, Bist P, Bi X, Pereira NA, Liu C, Sukumaran B, Rénia L, Ito Y, Lam KP. 2015. Bruton's tyrosine kinase phosphorylates DDX41 and activates its binding of dsDNA and STING to initiate type 1 interferon response. Cell Rep 10:1055–1065. https://doi.org/10.1016/j.celrep.2015.01.039.
31. Jiang LJ, Zhang NN, Ding F, Li XY, Chen L, Zhang HX, Zhang W, Chen SJ, Wang ZG, Li JM, Chen Z, Zhu J. 2011. RA-inducible gene-I induction augments STAT1 activation to inhibit leukemia cell proliferation. Proc Natl Acad Sci U S A 108:1897–1902. https://doi.org/10.1073/pnas.1019059108.
32. Cool J, DeFalco TJ, Capel B. 2011. Vascular-mesenchymal cross-talk through Vegf and Pdgf drives organ patterning. Proc Natl Acad Sci U S A 108:167–172. https://doi.org/10.1073/pnas.1010299108.